



4

5

6

10

11

13

14

15

16

17

18

19 20

21

22

23

25

26

27

28

29

30

31

32

33

34

35

36

37

38

39

40

41

Article

# Analysis of Nucleation and Glass Formation by Chip Calorimetry

Meng Gao<sup>1</sup>, Chengrong Cao<sup>1</sup> and John H. Perepezko<sup>1</sup>, \*

- <sup>1</sup> University of Wisconsin-Madison, Department of Materials Science and Engineering, 1509 University Ave. Madison, WI 53706; perepezk@engr.wisc.edu
- \* Correspondence: perepezk@engr.wisc.edu; Tel.: +1 (608)2631678 (JHP)

Featured Application: Authors are encouraged to provide a concise description of the specific application or a potential application of the work. This section is not mandatory.

**Abstract:** The advent of chip calorimetry has enabled an unprecedented extension of the capability of differential scanning calorimetry to explore new domains of materials behavior. In this paper, we highlight some of our recent work: the application of heating and cooling rates above  $10^4$  K/s allows for the clear determination of the glass transition temperature,  $T_g$  in systems where  $T_g$  and the onset temperature for crystallization,  $T_x$  overlap, the evaluation of the delay time for crystal nucleation, the discovery of new polyamorphous materials and the in-situ formation of glass in liquid crystals. From these application examples it is evident that chip calorimetry offers a promising potential to explore new reaction and transformation behavior and to develop new understanding.

**Keywords:** Chip calorimetry; Glass transition; Nucleation kinetics; Delay time; Polyamorphism; Amorphous materials, Liquid crystal

#### Citation:

Academic Editor: Firstname Lastname

Received: date Accepted: date Published: date

**Publisher's Note:** MDPI stays neutral with regard to jurisdictional claims in published maps and institutional affiliations.



Copyright: © 2021 by the authors. Submitted for possible open access publication under the terms and conditions of the Creative Commons Attribution (CC BY) license (https://creativecommons.org/licenses/by/4.0/).

1. Introduction

In many materials processing technologies, the thermal history involves various heating and cooling cycles as well as isothermal treatment. With the treatment of bulk components, the rate of heating and cooling is limited and is not constant throughout the volume. While the thermal history can be calculated by a heat flow analysis, the non-uniform thermal history can yield microstructural gradients and varying properties that confound accurate measurements. By a careful design of the thermal protocol and reduced sample volumes a uniform thermal history can be attained to enable the use of standard calorimetry techniques to measure material properties accurately. However, the standard techniques only allow for a limited heating and cooling rate of less than a few K/s. The recent advances in chip calorimetry have circumvented this limitation and allow for unprecedented rates of 2-5X10<sup>4</sup> K/s which has vastly expanded the capability of calorimetry to examine thermally activated reactions and phase transformations.

In this paper the application of chip calorimetry is demonstrated for the examination of glass transition temperature  $T_g$  and crystallization of metallic glass (MG) and amorphous polymers, and the development of polyamorphism as well as glass formation in liquid crystals. In each case the unique capability of chip calorimetry has enabled the exploration of new and novel transformation behavior that has permitted the development of new understanding.

#### 2. Materials and Methods

**Metallic glass samples.** The ingots of the compositions of Al<sub>92</sub>Sm<sub>8</sub> and La<sub>60</sub>Ni<sub>15</sub>Al<sub>25</sub> were prepared by arc melting the elemental components for several times in a Ti-gettered

argon atmosphere to ensure the homogeneity. For the Mg65Cu25Gd10 alloy, the ingot was prepared by an induction melting method in an argon atmosphere. Then, the ribbon-like samples were prepared by single-rolling melt spinning on a copper wheel with a tangential speed of 55 m/s. The thickness and the width of the ribbon-like samples were about 20X2 µmXmm. The melt spinning process was performed in inert argon gas. The structure of these as-cast samples and the annealed samples was characterized by X-ray diffraction . Meanwhile, the thermal properties of the above samples were measured by conventional diamond DSC (Perkin Elmer). The TEM tests were conducted on a Tecnai T12 instrument at 120 kV. The in-situ continuous heating, annealing treatment and the following thermal analyses were performed on a high-rate Flash DSC platform (Flash DSC2, Mettler Toledo) with chip sensor (UFS1). TEM samples from the annealed Flash DSC samples were prepared by Zeiss Auriga Focused Ion Beam (FIB) with a 10 nA FIB current and a 2 kV voltage to avoid sample damage.

**Polybutylene terephthalate (PBT) sample.** The commercial PBT film-like specimen was purchased from Sigma-Aldrich Co. (Product number is GF14031447). The thickness is 0.55 mm, and the melting temperature is about 250 °C. For PBT, the critical cooling rate for glass formation is about 1000 K/s [1]. To prepare the totally amorphous sample, one tiny piece was cut from the film-like commercial specimen and then was placed on the sample area of the chip sensor. The small piece firstly was heated into 270 °C and then was cooled down with the cooling rate of 10<sup>4</sup> K/s. The obtained amorphous sample was subjected to a series of annealing treatments with different annealing times under the same annealing temperature.

**D-mannitol sample.** D-mannitol (Aldrich, > 99%) was used as received. If cooled rapidly enough (> 30 K/s), the supercooled liquid (SCL) avoids crystallization, entering the glassy state below the  $T_g$  of 284 K (the glass transition temperature  $T_g$ ) [2, 3]. Before measurement, the sample was heated to 15 K above the melting point (440 K) for 10 s to allow the development of good contact with the detector chip. The schedule for a typical Flash DSC measurement, involves melting (100 K/s heating to 455 K), quenching (10³ K/s cooling to 223 K), annealing at temperatures ranging from 288 K to 333 K with annealing times ranging from 0 s to  $10^4$  s, and quenching and reheating (100 K/s) to temperature above the melting point [4]. The calibration of each chip was performed by the manufacturer and further validated against the melting point of D-mannitol.

Itraconazole (ITZ) sample. The sample material – itraconazole (ITZ) was supplied by Alfa Aesar with purity greater than 99% and used without further purification. The starting material was completely crystalline with a melting point of 440 K. For ITZ it was recently reported that at slow cooling (generally slower than 10 K/min), the isotropic liquid transforms to a nematic phase and then to a smectic phase, and finally produces a smectic ordered glassy solid[5]. However, at fast cooling (from 0.5 K/s to 20 K/s), smectic ordering can be avoided altogether or avoided partially [5]. To further obtain different structural ordered glassy solids in situ, before measurement, the sample was heated to about 33 K above the melting point for 2 s to allow the development of good contact with the detector chip, then the molten sample was quenched at a series of cooling rate from 10 to  $10^4$  K/s. The subsequent reheating curve at  $10^3$  K/s was used to conduct the thermal analyses.

# 3. Results and discussions

3.1. Nucleation and primary crystallization

3.1.1. Separation of glass transition temperature and crystallization temperature by increasing heating rate in marginal Al-based MG

For most MG systems with good glass formation ability, the glass transition signal is strong enough to be detected in the heating DSC traces, which makes it possible to

95

96

97

98

99

100

101

102

103

104

105

106

107

108

109

110

111

112

113

114

115116117

118

119

120

121

measure the glass transition temperature and the supercooled liquid region by the conventional DSC method. However, for marginal MGs such as the Al-based MGs, the glass transition signal is prone to be overlapped by a primary crystallization for Al nanocrystals precipitation [6, 7]. Thus, the traditional DSC is not a good thermal analysis tool to observe the glass transition of Al-based MGs. On the other hand, considering that the glass transition and crystallization are significantly different kinetic processes, they should follow different evolution paths with different heating rates, so that the two kinetic signals should be separated under higher heating rates. Here, we take the typical Al<sub>92</sub>Sm<sub>8</sub> MG as an example. The conventional DSC with heating rate of 0.33 K/s was applied to measure the heat flow curve shown in Figure 1a. It is clear that the conventional DSC heat flow curve only displays the primary and secondary crystallization peaks as shown in Figure 1b and there is no clearly defined glass transition signal. In contrast, the maximum heating and cooling rates for high-rate Flash DSC instrument with chip sensors (Flash DSC1, Mettler Toledo) are 4\*104 and 4\*103 K/s and the temperature range is between -90 °C and 450 °C [8, 9]. The optical picture of tiny MG sample being loaded onto the Flash DSC chip is shown in Figure 1b and the inserted optical picture gives the ribbon-like Al-based MG sample. A series of Flash DSC heat flow curves corresponding to different heating rates from 50K/s to 1000K/s were measured as shown in Figure 1c. For all heating rates by Flash DSC, the Flash DSC heat flow curve exhibits both the obvious glass transition and crystallization signals marked by  $T_g$  and  $T_{X_1}$ .

To further study the dynamic properties of glass transition and primary crystallization for the Al<sub>92</sub>Sm<sub>8</sub> MG, the evolutions of  $T_g$  and  $T_{XI}$  with heating rate are analyzed based on

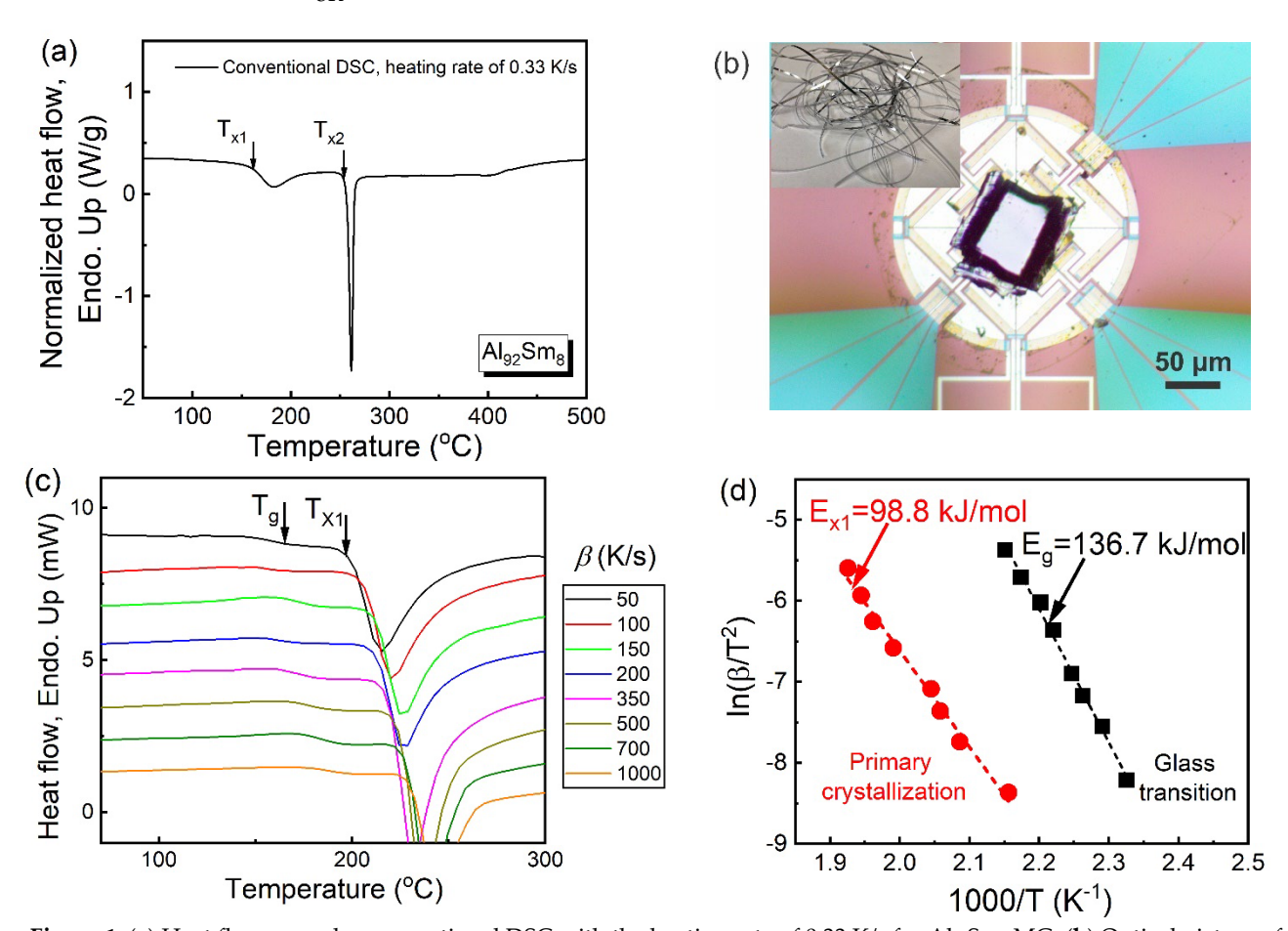


**Figure 1.** (a) Heat flow curve by conventional DSC with the heating rate of 0.33 K/s for Al<sub>22</sub>Sm<sub>8</sub> MG; (b) Optical picture of tiny MG sample on Flash DSC chip (the left inserted picture gives the optical photo of ribbon-like MG sample); (c) A series of Flash DSC heat flow curves by Flash DSC with the heating rates ranging from 50 to 1000 K/s; (d) Activation energies of glass transition and primary crystallization by fitting the experimental  $T_g$  and  $T_{XI}$  based on the Kissinger equation.

the Kissinger equation. For MGs, the glass transition temperature and the primary crystallization temperature usually follow the Kissinger equation [7]:

$$ln(\beta/T^2)=(-E/(RT))+constant$$
 (1),

where  $\beta$  is the heating rate, T is the value of the onset temperature of primary crystallization or the glass transition,  $E_g$  and  $E_{XI}$  are the activation energies for the glass transition and primary crystallization respectively and R is the gas constant. Thus, the activation energy for the glass transition and primary crystallization for Al<sub>92</sub>Sm<sub>8</sub> MG can be calculated by fitting the experimental results with Kissinger equation and the detailed results are shown in Figure 1d. The activation energy for primary crystallization is 98.8 kJ/mol and 136.7 kJ/mol for the glass transition. These activation energy values are comparable with those of previous researches in other Al-based MG systems [10-12]. Thus, for marginal Al-based MG, the glass transition requires a larger activation energy than that for the primary crystallization process. At a low heating rate in a conventional DSC, the  $T_g$ signal is superposed by the primary crystallization peak and the weak  $T_g$  signal is swallowed by the strong crystallization signal. With the increase of heating rates, both  $T_8$  and  $T_{X1}$  move to higher temperatures. However,  $T_g$  requires more activation energy to shift, and  $T_g$  will be left behind by  $T_x$ . Therefore, it is possible to discriminate the two signals and then determine the glass transition temperature for Al-based MGs. This result is consistent with the above observed glass transition signal in the Flash DSC heat flow curves with a series of fast heating rates in Figure 1c.

# 3.1.2. Delay time determination in various amorphous materials

An important application of amorphous materials is to serve as a precursor for the nucleation of crystalline phases that often develop with nanocrystalline sizes. The typical crystallization reaction is illustrated in figure 2a. Upon isothermal annealing, initially no crystals are present. During this delay time,  $\tau$  period crystalline embryos evolve with increasing size towards a critical size range where they can then proceed to grow as crystals. Within this delay time there is a transient nucleation as the equilibrium cluster size distribution is established to develop into a steady state nucleation rate. The steady state rate continues until a saturation of nucleation sites is reached and is then followed by a size coarsening regime. The transient nucleation rate, J(t), is represented by [13,14]

$$J(t) = J_{ssexp}[-\tau/t] \tag{2},$$

where t is the time and  $J_{ss}$  is the homogeneous nucleation that is given by

$$J_{ss} = \Sigma Z C_0 \exp[-\Delta G^*/kT]$$
(3),

where  $\Sigma$  is the atom attachment frequency to the evolving nucleation clusters, Z is the Zeldovich factor that has a typical value of 0.1,  $C_0$  is the nucleation site density,  $\Delta G^*$  is the work for nucleus formation, k is the Boltzmann constant and T is the temperature. Often  $\Sigma$  is taken as  $D/a^2$  where D is the bulk diffusivity and a is the atom spacing. Further since D is not always available it is estimated from the Stokes-Einstein relation

$$D = kT/[6\pi r \eta] \tag{4},$$

where  $\eta$  is the viscosity and r is the atom size. However, this approach has problems since the bulk diffusivity does not necessarily represent the interface attachment process governing cluster growth and it has been demonstrated that the Stokes-Einstein relation breaks down near  $T_g$  [15]. However, from nucleation theory there is a direct relation between  $\Sigma$  and  $\tau$  given by [14]

$$\Sigma = 1/2\tau Z^2 \tag{5}.$$

Thus, a measurement of  $\tau$  offers an accurate approach to evaluating  $\beta$  and the nucleation rate. Moreover, the magnitude of  $\tau$  also provides an effective evaluation of the glass formation ability as large  $\tau$  values are necessary for bulk glass formation. For example, a longer delay time at one temperature endows the higher thermal stability and the better glass formation ability, which is critical for developing bulk MGs [15]. Thus, it is of great importance to experimentally and precisely determine the delay time corresponding to different temperatures.

176

177

178

179

180

181

182

183

184

185

186

187

188

189

190

191

192

193

194

195

196

197

198

199

200

There are two common methods to experimentally measure the delay time for primary crystallization in amorphous materials: I. TEM method by plotting the measured crystal number density and the annealing time at one temperature and then extrapolating the steady state nucleation slope line to the time axis, the delay time can be established (see Figure 2a) [16, 17]; II. Isothermal test method by holding the amorphous sample at one temperature and then observing the onset time for the crystallization reaction (see Figure 2b) [18, 19]. For the method I, a great deal of TEM sample preparation and testing is required and thus it is very time-consuming, which is not a preferential method. For method II, the crystallization signal should be strong enough to show up in the isothermal annealing DSC trace, which makes it possible to directly measure the delay time for crystallization by isothermal tests. Thus, the amorphous system should have a good glass formation ability and thermal stability, such as the Zr-, Pd- and Ce-based bulk MG systems [18, 19]. However, for some marginal amorphous materials, such as the typica marginal Al-based MGs with poor glass formation ability, there usually appears a primary nucleation peak for Al nanocrystals followed by secondary or tertiary crystallization reactions involving intermetallic phases [20]. The signal from the primary nucleation of the precipitation of FCC Al nanocrystals is so weak that the crystallization peak is difficult to detect in the isothermal DSC tests [21]. Therefore, one precise and convenient method would be valuable for the determination of delay time for crystal nucleation in various amorphous materials.

Based on the Flash DSC with ultrafast heating and cooling rates, a new method is demonstrated to decide the delay time for primary crystallization. Under isothermal treatment, the evolution of glass transition temperature with annealing time for amorphous materials should follow two different paths: structural relaxation before the onset of crystal nucleation and the composition or ordering change after the onset of crystallization. Thus, the break time point in the slope of the plot of the glass transition temperature change with annealing time should correspond to the delay time for the primary crystallization [22, 23]. Three different kinds of amorphous systems were selected to verify the effectiveness and universality of the method, including one typical marginal Al-based MG with poor glass formation ability (Al<sub>92</sub>Sm<sub>8</sub>), two stable MG systems with good glass formation ability (La<sub>60</sub>Ni<sub>15</sub>Al<sub>25</sub> and Mg<sub>65</sub>Cu<sub>25</sub>Gd<sub>10</sub>) and one amorphous polymer (Polybutylene terephthalate, PBT)).

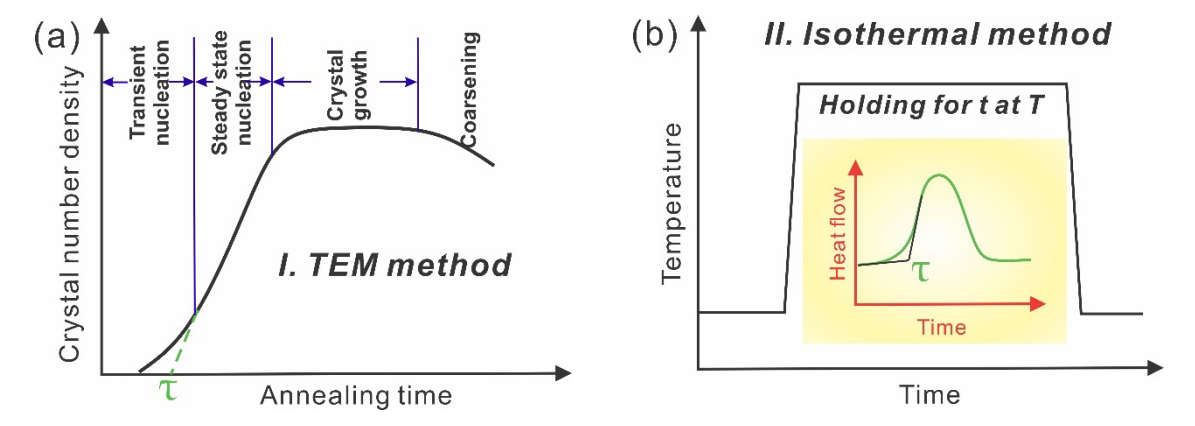


Figure 2. Schemes of traditional experimental methods to determine the delay time  $\tau$  for primary crystallization in MGs: (a) TEM method (I); (b) Isothermal method based on the thermal tests (II). The inserted graph in (b) gives the confirmation details of delay time by method II.

# 3.1.2.1. Marginal Al-based MG

For the conventional DSC with heating rate of several K/s, the thermal signal of the glass transition for marginal Al-based MGs cannot be detected due to the close overlap of

201202203204205206207

208

209

210211212213214215

218 219 220

216

217

221222

the strong crystallization exotherm. In contrast, the Flash DSC with the large heating rate range from several K/s to  $10^4$  K/s allows for the separation of the  $T_g$  and  $T_x$  signals, as described in part 3.1.1. Thus, the ultrafast chip calorimetry instrument provides a good opportunity to study the delay time for marginal Al-based MGs. For an Al<sub>92</sub>Sm<sub>8</sub> MG, a series of Flash DSC heat flow curves with the same heating rate of 1000 K/s was measured after annealing at 150°C for different times ranging from 20 s to 10000 s, as shown in Figure 3a. It is obvious that all of Flash DSC heat flow curves display the obvious endothermic reaction signals corresponding to glass transition and the T<sub>8</sub> shifts to the higher temperature with the increase of annealing time  $t_a$ . These results are very close to the previous research on the structural relaxation effect on MGs [24, 25]. To study the evolution of the glass transition temperature  $T_g$  with annealing time  $t_a$ ,  $T_g$  is plotted against  $t_a$  at 150 °C, as is shown in the Figure 3b. From Figure 3b, it is evident that with the increase of t<sub>a</sub>, there appears one break point at 930 s. Before and after 930 s, the evolution paths of  $T_g$ with  $t_a$  can be roughly fitted by two lines with different slopes. These two different evolution paths correspond to the structural relaxation effect and the composition effect and the samples before and after the break points should be amorphous and contain nanocrystals, respectively [22, 23].

To further test if the delay time for primary crystallization corresponds to the experimental breaking time of glass transition temperature with annealing time, two annealing time points were selected before and after the breaking time,  $t_1$  (550 s) and  $t_2$  (1200 s). Then, for these two annealed samples by Flash DSC, TEM samples were prepared by FIB methods in order to observe the corresponding crystallization morphology. The corresponding TEM images corresponding to  $t_1$  and  $t_2$  are shown in Figure 3c and Figure 3d, respectively. It is evident that at 150 °C, the sample with the annealing time of 550 s before the break

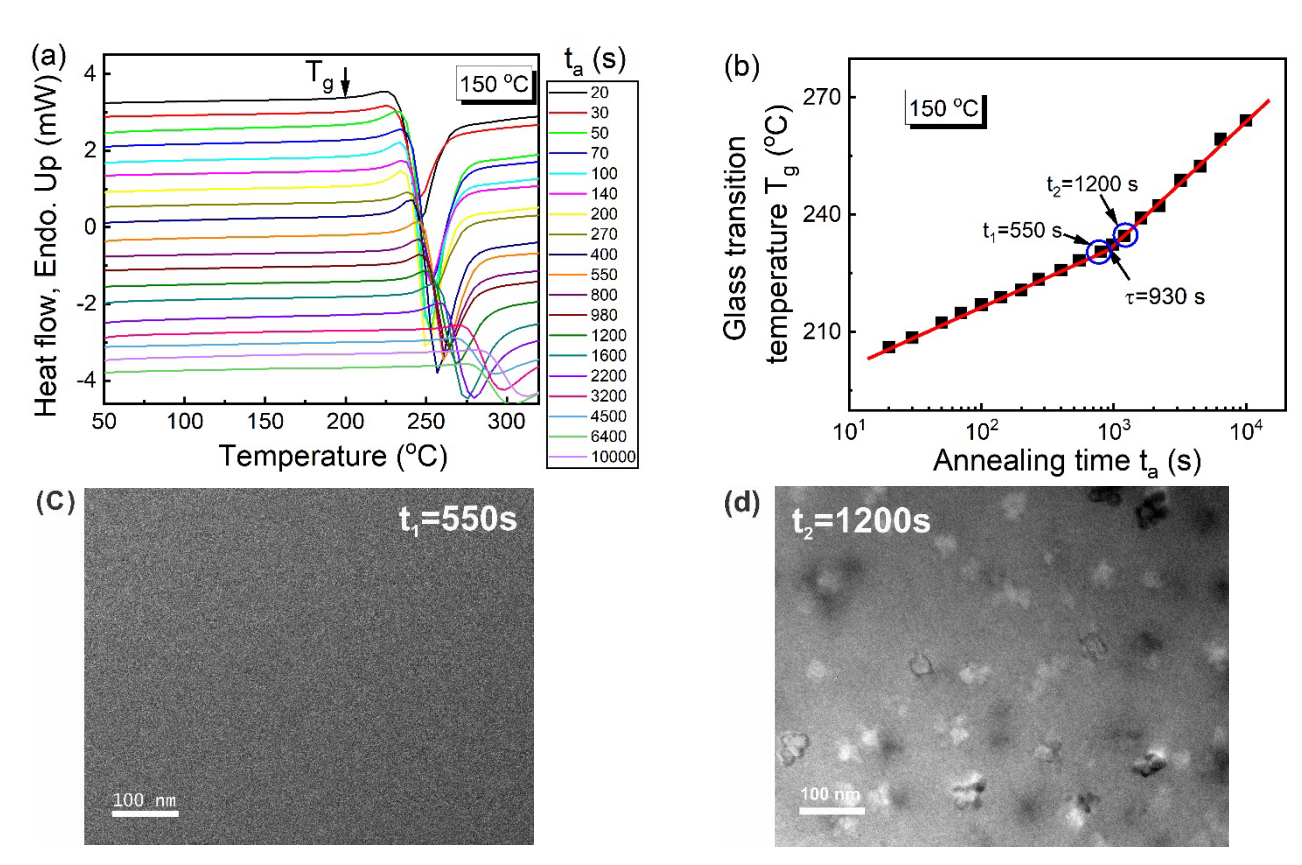


**Figure 3.** (a) A series of Flash DSC heat flow curves corresponding to different annealing times ranging  $t_a$  from 20 to 10000 s at 150 °C for Al<sub>2</sub>Sm<sub>8</sub> MG; (b) Plot of  $T_g$  and  $t_a$  at 150 °C ( $t_1$  and  $t_2$  are two selected annealing times before and after the break point of 930 s); (c) TEM image for annealed sample corresponding to the annealing time of  $t_1$ ; (d) TEM image for annealed sample corresponding to the annealing time of  $t_2$ .

point is still amorphous without any crystals; in contrast, for the samples with the annealing time of 1200 s after the break point, a great number of nanoscale crystals are observed. Thus, the above results and analyses verify that the break point of 930 s is actually the delay time at 150 °C for the Al<sub>92</sub>Sm<sub>8</sub> MG, which is consistent with previous research [22, 23].

# 3.1.2.2. Stable La-based MG

For the stable La-based MG system, the thermal signals for the glass transition and primary crystallization are strong [26]. To verify if the above new method to confirm the delay time for primary crystallization is effective for the La-based MG, one typical composition of La60Ni15Al25 was selected and the target temperature was set of 270 °C Then, a series of Flash DSC heat flow curves corresponding to different annealing times ranging from 1 s to 50 s with the heating rate of 500 K/s were measured, as shown in Figure 4a. From Figure 4a, the heat flow curves with different annealing times for La60Ni15Al25 MG exhibit the obvious signals of the glass transition and primary crystallization. The onset values of the glass transition obviously shift to the higher temperature range with the increase of the annealing times, which is consistent with the structural relaxation effects in MGs [24, 25]. Similar to the analyses process for the delay time confirmation method in part 3.1.2.1 for Al-based MG, the onset value of the glass transition  $T_g$  with the annealing time  $t_a$  can be plotted as shown in Figure 4b. From Figure 4b, it is apparent that with the increase of  $t_a$  at 270 °C, there appears a break point time at 22.5 s. Before and after 22.5

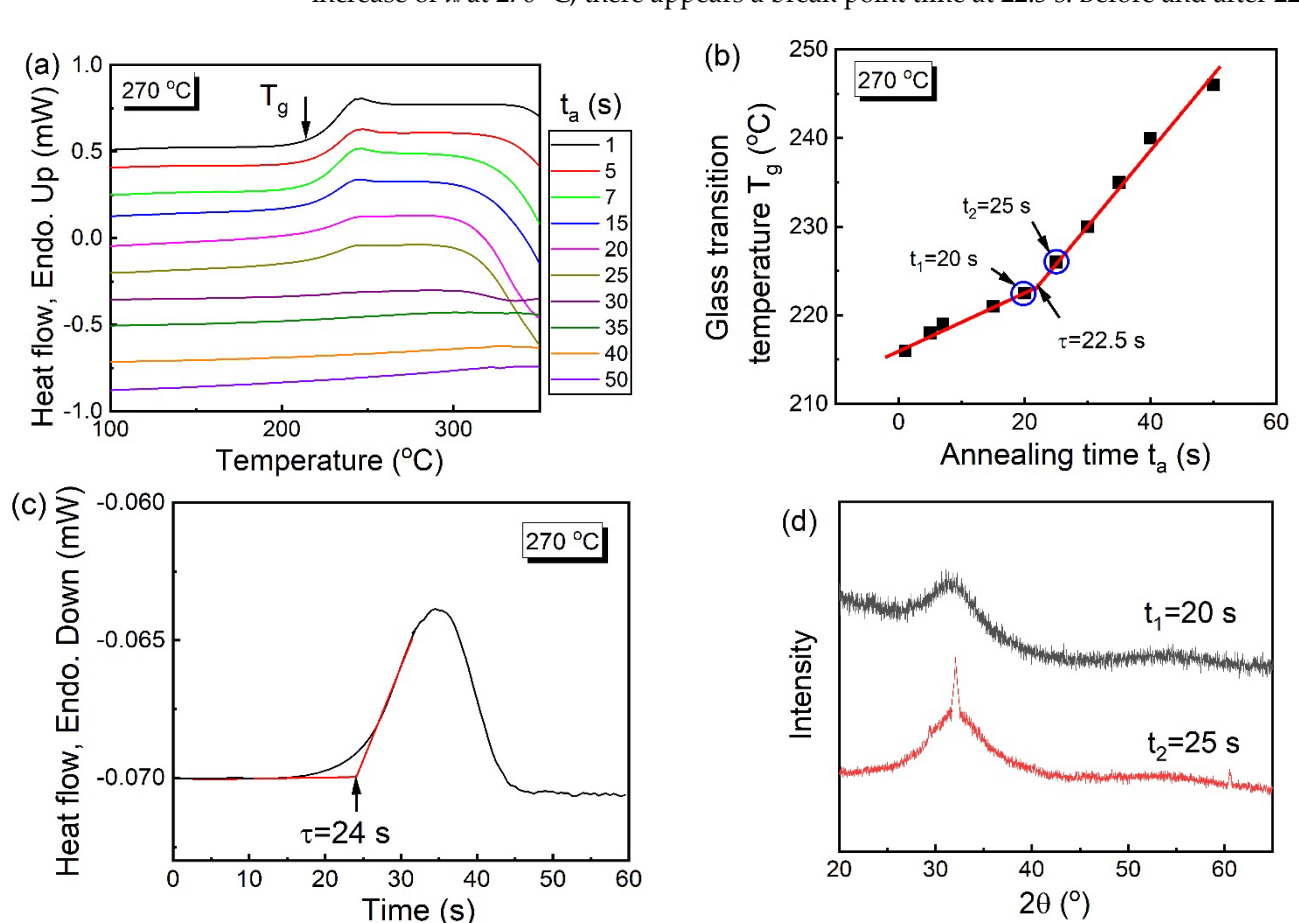


**Figure 4.** (a) A series of Flash DSC heat flow curves corresponding to different annealing times ranging  $t_a$  from 1 to 50 s at 270 °C for La<sub>60</sub>Ni<sub>15</sub>Al<sub>25</sub> MG; (b) Plot of  $T_g$  and  $t_a$  at 270 °C ( $t_1$  and  $t_2$  are two selected annealing times before and after the break point of 22.5 s); (c) The isothermal test for La<sub>60</sub>Ni<sub>15</sub>Al<sub>25</sub> MG at 270 °C; (d) XRD patterns for annealed samples corresponding to the annealing times of  $t_1$  and  $t_2$ .

s, the evolution paths of  $T_8$  with  $t_a$  can be roughly fitted by two lines with different slopes corresponding to two different governing mechanism of the structural relaxation and the composition change induced by the crystallization. In comparison, the isothermal method (method II in Figure 2b) was also applied to measure the delay time for La<sub>60</sub>Ni<sub>15</sub>Al<sub>25</sub> MG sample at 270 °C. The detailed temperature program can be seen in Figure 2b. As shown in Figure 4c, at 270 °C, when the annealing time increases into about 24 s, the exothermic peak corresponding to the primary crystallization appears. The time of 24 s is the delay time at 270 °C, which is very close to the experimental data of 22.5 s by the Flash DSC method.

To confirm if the delay time of the experimental breaking time of glass transition temperature with annealing time in Figure 4b corresponds to the onset time for primary crystallization, two annealing time points were selected before and after the break time,  $t_1$  (20 s) and  $t_2$  (25 s). Then, for these two annealed samples obtained by Flash DSC, XRD tests were conducted to characterize the sample state. The corresponding XRD patterns corresponding to the annealing times of  $t_1$  and  $t_2$  are shown in Figure 4d. It is apparent that at 270 °C, the sample with the annealing time of 20 s before the break point is still amorphous without any crystals; in contrast, for the samples with the annealing time of 25 s after the break point time, one sharp crystallization peak was observed, which indicates that the annealed sample is crystallized. Thus, the above results show that the break point time of 22.5 s is actually the delay time at 270 °C for the stable La<sub>60</sub>Ni<sub>15</sub>Al<sub>25</sub> MG.

# 3.1.2.3. Stable Mg-based MG

Similar to the stable La-based MG, the Mg-based MG with a composition of Mg65Cu25Gd10 is also one of the typical stable MG systems [27]. As shown in Figure 5a, a series of Flash DSC heat flow curves were obtained corresponding to different annealing times ranging

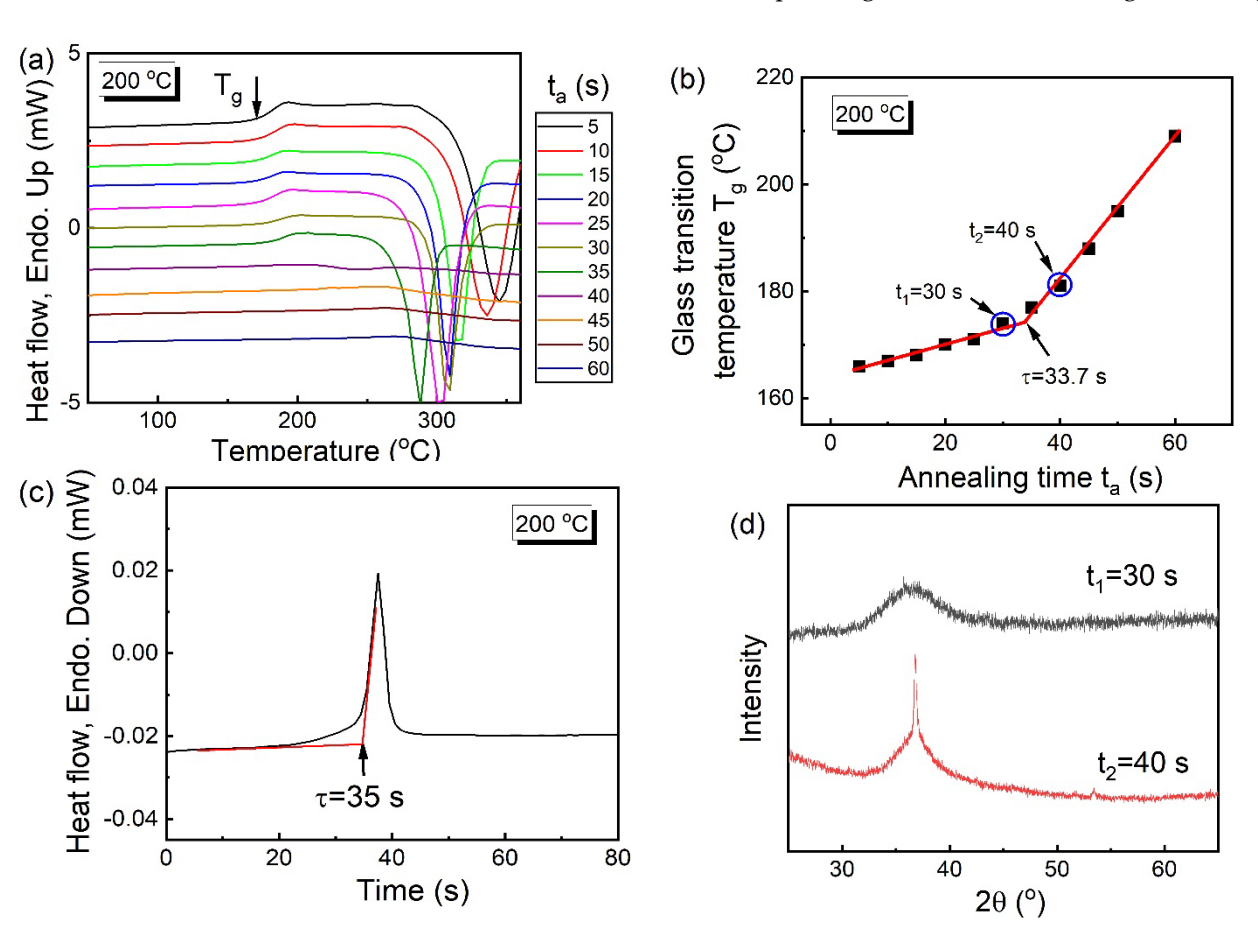


**Figure 5.** (a) A series of Flash DSC heat flow curves corresponding to different annealing times ranging  $t_a$  from 5 to 60 s at 200 °C for Mg<sub>65</sub>Cu<sub>25</sub>Gd<sub>10</sub> MG; (b) Plot of  $T_g$  and  $t_a$  at 200 °C ( $t_1$  and  $t_2$  are two selected annealing times before and after break point of 33.7 s); (c) The isothermal test for Mg<sub>65</sub>Cu<sub>25</sub>Gd<sub>10</sub> MG at 200 °C; (d) XRD patterns for annealed samples corresponding to the annealing times of  $t_1$  and  $t_2$ .

from 5 s to 60 s at 200°C with the heating rate of 500 K/s. The heat flow curves with different annealing times for Mg65Cu25Gd10 MG exhibit the clear signals of the glass transition and primary crystallization, which are consistent with the thermal behaviors for La-based MG in part 3.1.2.2. What is more, the  $T_g$  shifts to the higher temperature with the increase of the annealing time  $t_a$ . Similar to the analyses process for the delay time confirmation method in part 3.1.2.1 for Al-based MG and in part 3.1.2.2 for La-based MG, the onset value of the  $T_g$  with the annealing time  $t_a$  can be plotted as shown in Figure 5b. From Figure 5b, with the increase of  $t_a$  at 200 °C, there appears one break point time at 33.7 s. Before and after 33.7 s, the evolution paths of  $T_g$  with  $t_a$  follows two different paths corresponding to the structural relaxation and the composition effect. Meanwhile, the isothermal method was also applied to measure the delay time for Mg65Cu25Gd10 MG sample at 200 °C. As shown in Figure 5c, at 200 °C, when the annealing time increases into about 35 s, the exothermic peak corresponding to the primary crystallization appears. The time of 35 s is the delay time at 270 °C, which is very close to the experimental data of 33.7 s based on the evolution of the glass transition  $T_g$  with the annealing time  $t_a$ .

To confirm if the delay time of the experimental breakpoint time by Flash DSC corresponds to the onset time for primary crystallization, two annealing time points were selected before and after the break point time,  $t_1$  (30 s) and  $t_2$  (40 s). XRD tests for these two annealed samples were conducted. The corresponding XRD patterns corresponding to the annealing times of  $t_1$  and  $t_2$  were shown in Figure 5d. One can see that at 200 °C, the sample with the annealing time of 30 s before the breakpoint time are still amorphous without any crystals; in contrast, for the samples with the annealing time of 40 s after the breakpoint time, one sharp crystallization peak was observed. Thus, the above results show that the break point time of 33.7 s is actually the delay time at 200 °C for the stable Mg65Cu25Gd10 MG.

# 3.1.2.4. Amorphous polymer material

To verify if the delay time confirmation method by Flash DSC can be applied for the amorphous polymer materials, one typical amorphous polymer-polybutylene terephthalate (PBT) was chosen for examination [1, 29]. At an annealing temperature of 50 °C, a series of heat flow curves with different annealing times ranging from 2 s to 12 s were measured and are shown in Figure 6a. Similar to the MG systems, the glass transition temperature  $T_g$  for PBT sample also shifts to the higher temperature with the increase of the annealing time  $t_a$ , which indicates the structural relaxation effect. Moreover, the corresponding  $T_g$ - $t_a$ dependence can be plotted in Figure 6b. When t<sub>d</sub> increases into about 6.6 s, a break point appears between the two evolution paths. Meanwhile, the isothermal method was also applied to measure the delay time for PBT sample at 50 °C. As shown in Figure 6c, at 50 °C, when the annealing time increases into about 6.3 s, the exothermic peak corresponding to the primary crystallization appears. The time of 6.3 s is the delay time at 50 °C, which is very close to the experimental data of 6.6 s based on the evolution of the glass transition  $T_g$  with the annealing time  $t_a$ . By selecting three annealing time points before  $(t_1, 6 \text{ s})$  and after the break point  $(t_2, 8 s)$ , the XRD tests for these two annealed samples were conducted. The annealed samples before and after break point are respectively amorphous and crystalline in Figure 6d, which confirms the delay time at 50 °C for the PBT sample. Based on the previous research [28], for amorphous polymer materials, with the increase of the annealing time, the crystalline phase gradually grows and the ordering degree within polymer increases. Considering that the polymer is one single composition, the break point for  $T_g$ - $t_a$  plot in amorphous PBT in Figure 6b corresponds to the transition from the relaxation effect to the ordering effect.

Based on the above results and discussions in parts 3.1.2.1-3.1.2.4, the experimental method to determine the delay time for primary crystallization based on the chip calorimetry is an effective method for various amorphous materials, which provides a good opportunity to investigate the nucleation and crystallization behaviors in glassy materials.

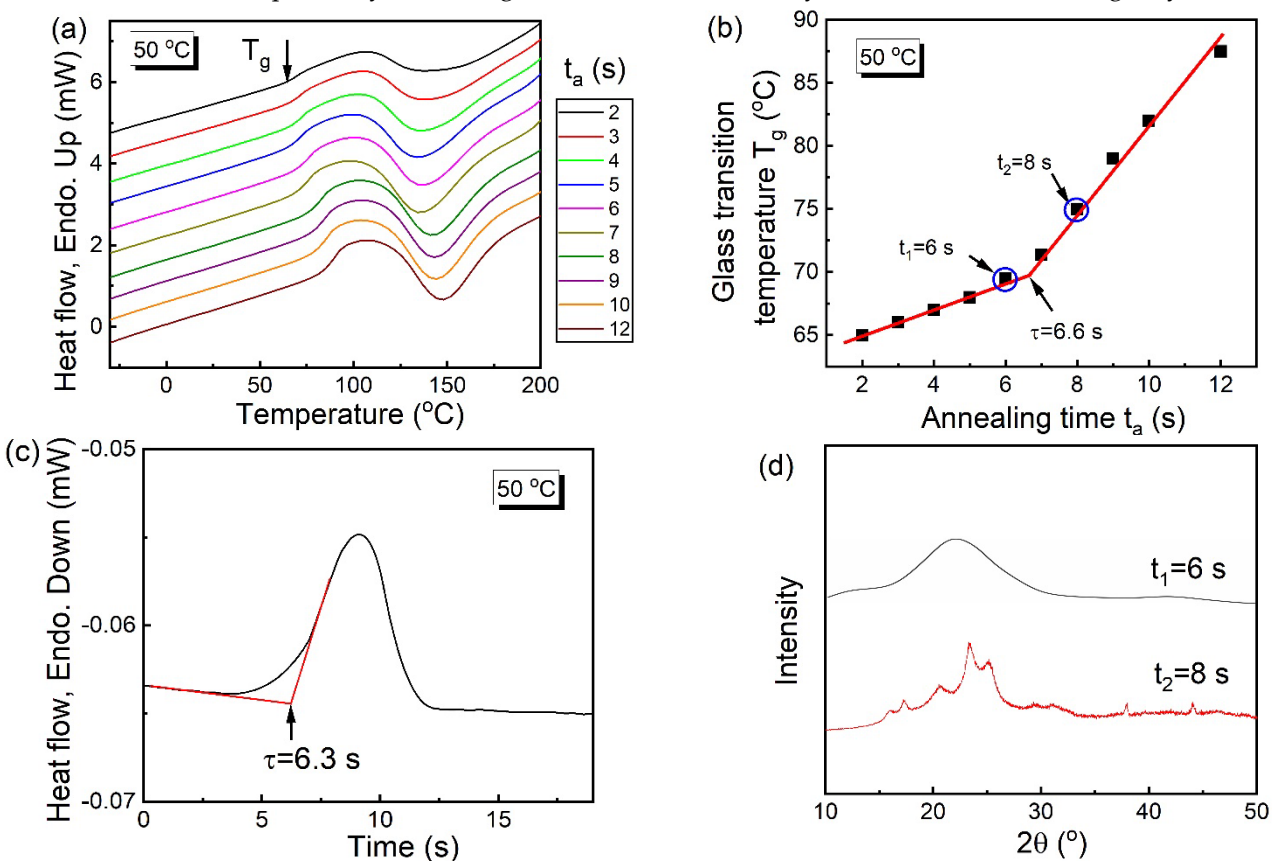


**Figure 6.** (a) A series of Flash DSC heat flow curves corresponding to different annealing times ranging  $t_a$  from 2 to 12 s at 50 °C for amorphous PBT sample; (b) Plot of  $T_g$  and  $t_a$  at 50 °C ( $t_1$  and  $t_2$  are two selected annealing times before and after the break point of 6.6 s); (c) The isothermal test for PBT sample at 50 °C; (d) XRD patterns for annealed samples corresponding to the annealing times of  $t_1$  and  $t_2$ .

#### 3.2. Glass formation

# 3.2.1. New polyamorphous material-D-mannitol

Polyamorphism refers to the existence of two amorphous phases of the same composition separated by a first-order transition. This phenomenon is analogous to crystal polymorphism exemplified by diamond and graphite but is less well understood and even controversial [30]. Zhu *et al.* reported that the melt-quenched glass of D-mannitol can transit into another apparently amorphous state by continuous heating or isothermal annealing, with a first-order characteristic [2]. In agreement with this report, the first-order transition can be completed by annealing the melt-quenched sample at 310 K for 180 s in the conventional DSC. Figure 7a shows when heating the melt-quenched glass (GN) sample with a 20 K/min heating rate, the sample begins the glass transition to a supercooled liquid (SCL-1) at 287 K, but further heating results in an exothermic transition from SCL-1 to amorphous phase X (GX) beginning at 298 K. When heating a sample that has been aged at 310 K for 180 s, the sample shows neither a glass transition at 287 K nor a sharp exothermic peak at 298 K [3]. This is identical to the DSC heating trace of the GX sample which is obtained by first being heated to 313 K (above the first exothermic transition) and then quenched [2].

The X-ray diffraction patterns of GN, GX, and the  $\alpha$  crystal polymorph are shown in Figure 7b It is evident that GX does not have crystal-like diffraction features, which strongly indicates that the GX is an amorphous state. Also, the diffraction pattern of GX is distinct from that of GN. The GX has a featured broad maximum that appears at lower 2 $\theta$  than that for the GN, with an additional small peak around 15 $^{\circ}$ , which likely results from a different local structure with long range correlation. This is consistent with the report that the GN has a smaller specific volume than GX at 273 K, which is the measuring temperature of the X-ray diffraction experiments [3, 4].

Due to the slow heating rates of the conventional DSC, GX can form from SCL-1 of GN to produce an exothermic peak. In the Flash-DSC, however, the 100 K/s or even a 10 K/s heating rate is too fast to allow for this transition so that no exothermic peak can be observed on the heating trace of a melt-quenched GN sample. On the other hand, if the GN sample is annealed with a combination of annealing temperature that can trigger the GN/SCL-1 to GX transition and annealing time that is longer than the delay time of the transition, GX can be formed in the annealed sample and the glass transition of GX can appear in the following heating trace.

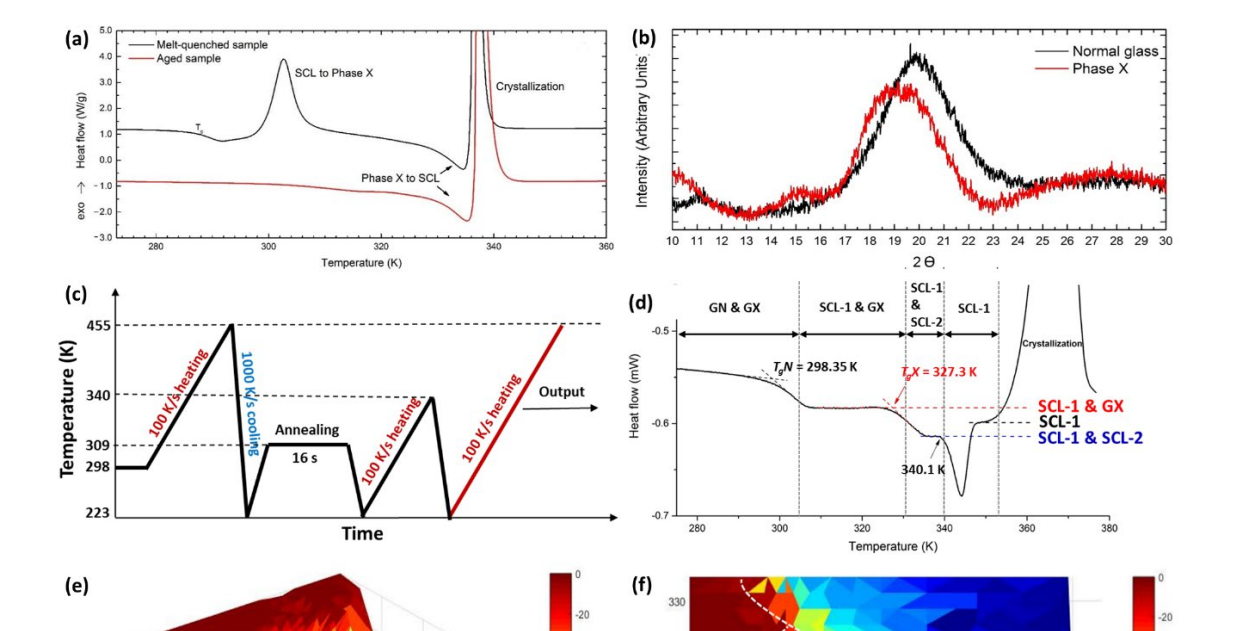


**Figure 7.** (a) Conventional DSC measurements on a normal glass (GN) and a phase X (GX) D-mannitol sample[31, 33]. (b) X-ray diffraction patterns of GN and GX[31, 33]. (c) The experimental protocol for the sample preparation in (d). (d) Transition path during heating. Sample was annealed at 309 K for 16 s, preheated to 340 K and quenched down before this heating. Sample starts as a mixture of normal (melt-quenched) glass and phase X, and shows 3 endothermic transitions: (1) glass transition of GN (298 K); (2) glass transition of GX (328 K); (3) liquid-liquid from SCL-2 to SCL-1 (340 K)[33]. (e) and (f) Enthalpy change with different annealing conditions, (e) is 3-D plot of the enthalpy change with  $T_a$  and  $\ln(t_a)$ , (f) is the result of projecting the profile onto T-t plane, the boundaries between adjacent plateaus are the Time-Temperature-Transition curves of the corresponding transition[33].

An example of that protocol is shown in Figure 7c. After an anneal at  $T_a$  = 309 K and annealing time  $t_a$  = 16 s, the sample is then reheated to 340 K to obtain the supercooled liquid state and immediately quenched. The following heating trace in Figure 7d clearly shows three endothermic transitions before crystallization as  $T_g$  of GN at 298.3 K,  $T_g$  of GX at 327.3 K and the transition from SCL-2 to SCL-1 at 340.1 K. It is also worth noting that the mixture of SCL-1 and SCL-2 has a larger specific heat capacity than that for pure SCL-1, which means that pure SCL-2 has a larger specific heat value compared to pure SCL-1[4].

By choosing the Flash-DSC heating trace of the unannealed GN sample as a baseline that is subtracted from each of the annealing traces, the enthalpy changes under each annealing condition can then be calculated by integrating the remaining curve from Ta to 458 K. By normalizing the enthalpy change with the corresponding sample weight, a three-dimensional plot of the enthalpy change with  $T_a$  and  $ln(t_a)$  can be constructed as shown in Figure 7e. There are three plateaus in the 3-D profile, which correspond to unannealed GN/SCL-1 ( $\Delta H = 0$  J/g red), GX/SCL-2( $\Delta H = -50$  to -65 J/g, yellow and orange), and  $\alpha$  crystalline ( $\Delta H = -160 \text{ J/g}$ , blue), respectively. Figure 7f is obtained by projecting the three-dimensional surface onto the T-ln(t) plane. In this projection, the boundaries between adjacent plateaus are actually the Time-Temperature-Transition (TTT) curve. The transition boundary between the two amorphous states has a C shape, which is a main feature of thermally activated phase transitions. As a consequence, the time length to reach the boundary at a certain temperature is the delay time  $\tau$  for the reaction. It can also be seen that, although the difference is not very large, the height of the plateau corresponding to GX formed at lower annealing temperature (below 305 K) is greater than that formed at higher annealing temperature [4].

# 3.2.2. In-situ formation of glass in liquid crystals

Liquid crystals (LCs) usually are known to undergo rapid ordering transitions with virtually no hysteresis. These transitions are so fast that nearly no supercooling can be observed under ordinary conditions. This allows LCs to serve as standards for temperature calibration at fast cooling rates (up to  $2 \times 10^4 \, \text{K/s}$ ) [31, 32]. Recently, ITZ was reported as an exceptional case. At slow cooling, the isotropic liquid transforms to a nematic phase and then to a smectic phase, but at fast cooling, smectic ordering can be avoided altogether

or avoided partially to produce glassy solids with variable smectic order [5]. To exhibit the smectic ordering in an equilibrium liquid of ITZ, Figure 8a shows that the isotropic liquid of ITZ transforms to a nematic phase ( $T_{N/l}$  = 363 K) and then to a smectic phase ( $T_{Sm/N}$  = 347 K) [33-35], In the nematic phase, the molecules are aligned with their long axes approximately parallel to each other, while in the smectic phase, the molecules are further organized into layers [5]. Further cooling transforms the smectic liquid to a glassy solid ( $T_g$  = 328 K). Upon reheating, the transitions noted above are reversible.

At different cooling rates ( $R_c$ ) ITZ glasses can be prepared with and without smectic order. When the cooling rate faster than the relaxation of nematic to smectic transition so that at  $R_c > 20$  K/s ITZ can be free of smectic order [5]. The rates of molecular rotations in a liquid crystal can be obtained by dielectric spectroscopy as shown in Figure 8b [36]. Similar to other LCs [37-39], ITZ shows two relaxation processes[40, 41]. The fast process has been associated with the glass transition detected by DSC[38, 40] and is termed the  $\alpha$  process , where the  $R_c$  value for glass formation is given by the right axis in Figure 8b. This process is attributed to molecular rotation about the long axis and precession of the long axis about the nematic director, whereas the slow process (called the  $\delta$  mode) is attributed to molecular rotation about the short axis (end over end). The rates of the two processes can be significantly different in a liquid crystal; this is a result of a nematic potential that favors the alignment of the long axis along the director and reduces the average rate of end-over-end rotation [5].

From Figure 8b it is evident that if  $R_c > 10^3$  K/s which is even faster than the rate of the isotropic to nematic transition, the two LC transitions will be avoided, and the liquid can be directly quenched into glassy state. Therefore, to obtain the isotropic glass, the molten sample was quenched at a series of cooling rate from 10 to  $10^4$  K/s and then reheated at  $10^3$  K/s to determine the different quenched glassy state structures. Different from the heating curve measured by conventional DSC as shown in Figure 8a, at a high heating rate under Flash DSC the peak of glass transition overlaps with the peak of the smectic to nematic transition. The evolution of the profile of heating curve is guided by the dash line shown in Figure 8c. Even at the low heating rates from 10 to 100 K/min under

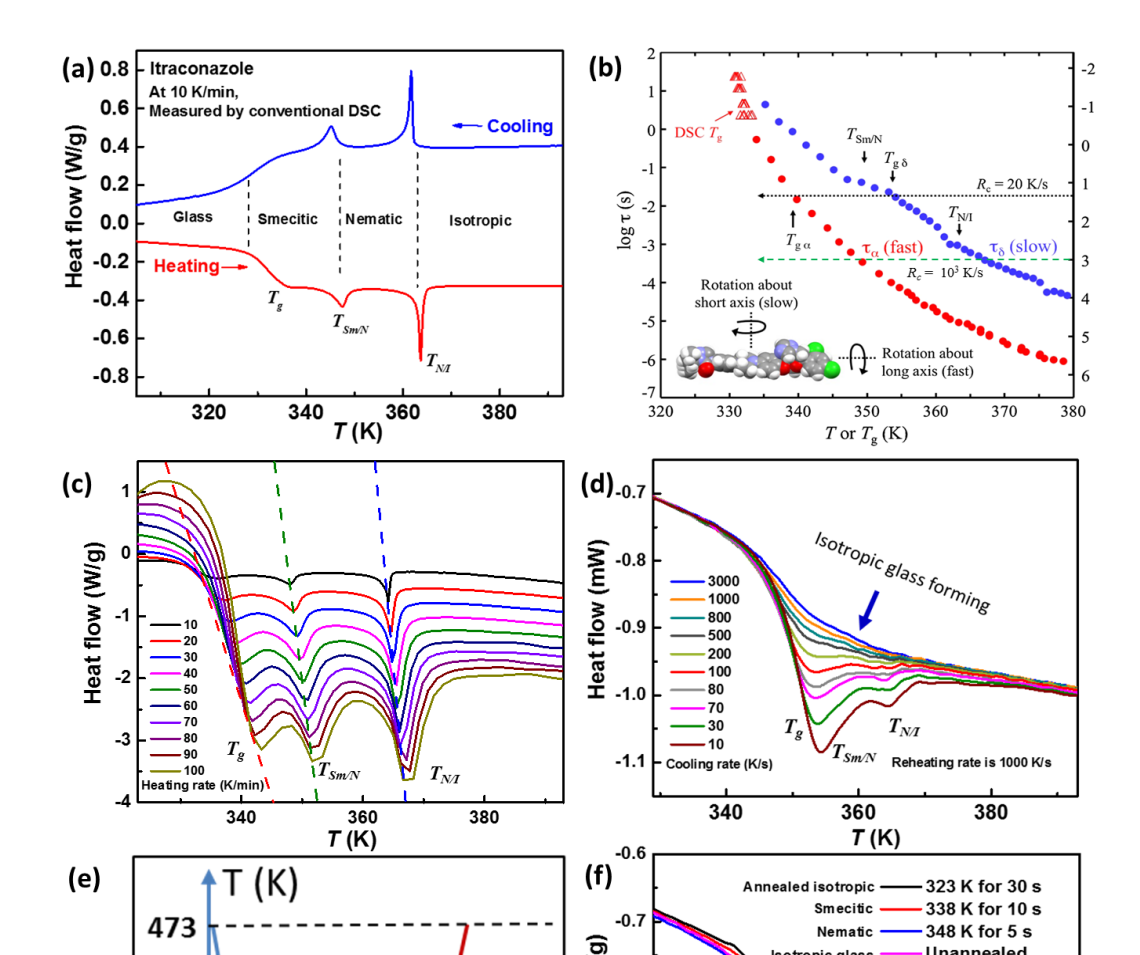


**Figure 8.** (a) Conventional DSC traces of ITZ during cooling and reheating at 10 K/min. (b) Fast (red circles) and slow (blue circles) relaxation processes in ITZ from dielectric spectroscopy[from Ref. 45], conventional DSC  $T_g$  onset (triangle) is shown as a function of cooling rate  $R_c$  (right axis)[34]. (c) A series of conventional DSC reheating traces with different heating rates, started from the melt quenched ITZ glass at 10 K/min cooling rate. (d) Flash DSC reheating curves with  $10^3$  K/s heating rate, the measured ITZ glass formed upon a series of cooling rates from 10 to  $3\times10^3$  K/s. (e) The experimental protocol for the different ITZ glass formation in (f). (f) Flash DSC reheating curves at  $10^3$  K/s heating rate, to examine the ITZ glassy state after the different annealing conditions.

conventional DSC, the endothermic hump signal of  $T_g$  shows the obvious tendency to merge with the peak of  $T_{Sm/N}$  while the distance between the peaks of  $T_{Sm/N}$  and  $T_{N/l}$  stays almost the same. Meanwhile the profile of the peaks smooths with increasing heating rate gradually. Therefore, for Flash DSC measurements see in Figure 8d, the reheating curves upon slow cooling ( $R_c < 100 \text{ K/s}$ ) show two apparent peaks about the overlapped  $T_g$  with  $T_{Sm/N}$  and then the small one about  $T_{N/l}$ . Consistent with the relaxation process in Figure 8b [5, 40], upon cooling at  $R_c > 500 \text{ K/s}$  in Figure 8d, there is only the glass transition without the signal of the LC transitions, which indicates that the isotropic to nematic transition was avoided during this fast cooling process to form the isotropic ITZ glass .

Since the highly disordered isotropic glass can be formed upon  $10^3$  K/s quenching, to obtain more kinds of ITZ glass, we conducted annealing treatments on the as-quenched sample according to the protocol shown in Figure 8e. The sample was annealed at 323 K ( $T_a > T_g$ ), 338 K ( $T_g < T_a < T_{Sm/N}$ ) and 348 K ( $T_{Sm/N} < T_a < T_{N/I}$ ) for sufficient time according to the relaxation process [5, 40], respectively. As a result, in Figure 8f the reheating curve of the sample annealed below  $T_g$  only shows one deep endothermic peak due to the aging effect of the glass which indicates that there was no apparent smectic or nematic order formed during annealing and sample remained in the isotropic glassy state. While for the higher  $T_a$  annealed samples, the red curve shows both endothermic peaks of the overlapped  $T_g$  with  $T_{Sm/N}$  and then  $T_{N/I}$ , indicating the formation of smectic layers during annealing. Then the blue curve only shows the obvious  $T_{N/I}$  and the weaker signal of  $T_g$  with  $T_{Sm/N}$  as a shoulder, indicating that the nematic to isotropic transition dominates in this heating process. Therefore, upon annealing in-situ the various LC orders can be effectively trapped in a glass at a  $10^3$  K/s cooling rate.

### 4. Conclusions

In this work, recent work is highlighted on nucleation and glass formation by chip calorimetry with ultrafast heating and cooling rate. First, for marginal Al-based MG system, based on the separated evolution of glass transition and primary crystallization with heating rates, the glass transition signal is successfully separated from primary crystallization within huge heating rate range. Second, one effective and universal method to experimental determine the nucleation delay time of primary crystallization based on the

e 636 s 637 n 638 o 639 t 640 n 641 o 643

chip calorimetry platform. This method has been verified to be applied for various amorphous materials including the marginal MG system, the stable MG systems and the amorphous polymer system. Third, results from flash DSC experiments provided insights into the characteristics of the amorphous-amorphous transition, in particular the precise annealing conditions that could be reached by flash DSC enabled the construction of the Temperature-Time-Transformation (TTT) plot of D-mannitol for the transition between GN/SCL-1 and GX/SCL-2, as well as the transition between amorphous and crystalline phases revealing thermally activated behavior. Fourth, for LC material ITZ, upon annealing in-situ the various of LC orders can be effectively trapped in a glass at a high cooling rate.

Author Contributions: Conceptualization, M.G., C.R.C. and J.H.P.; methodology, M.G. and C.R.C. ; software, M.G. and C.R.C.; validation, M.G., C.R.C. and J.H.P.; formal analysis, M.G., C.R.C. and J.H.P.; writing—original draft preparation, M.G., C.R.C. and J.H.P.; writing—review and editing, M.G., C.R.C. and J.H.P.; visualization, M.G., C.R.C. and J.H.P.; supervision, J.H.P.; project administration, J.H.P.; funding acquisition, J.H.P. All authors have read and agreed to the published version of the manuscript.

Funding: This research was funded by the Office of Naval Research (N00014-20-1-2704) and NSF (UW-Madison MRSEC DMR 1720415).

Acknowledgments: In this section, you can acknowledge any support given which is not covered by the author contribution or funding sections. This may include administrative and technical support, or donations in kind (e.g., materials used for experiments).

Conflicts of Interest: The authors declare no conflict of interest.

References 688

- Schawe, J. E. K. Influence of processing conditions on polymer crystallization measured by fast scanning DSC. J. Therm. Anal. Calorim. 2014, 116, 1165-1173.
- M. Zhu, J. Q. Wang, J. H. Perepezko, and L. Yu. Possible existence of two amorphous phases of D-mannitol related by a first-2. order transition. J. Chem. Phys. 2015, 142, 244504.
- M. Zhu and L. Yu. Polyamorphism of D-mannitol. J. Chem. Phys. 2017, 146, 244503. 3.
- W. Tang and J. H. Perepezko. Polyamorphism and liquid-liquid transformations in D-mannitol. J. Chem. Phys. 2018, 149, 074505.
- R. Teerakapibal, C. Huang, A. Gujral, M. D. Ediger, and L. Yu. Organic Glasses with Tunable Liquid-Crystalline Order. Phys. Rev. Lett. 2018, 120, 055502.
- 6. Bondi, K. S.; Gangopadhyay, A. K.; Marine, Z.; Kim, T. H.; Mukhopadhyay, A.; Goldman, A. I.; Buhro, W. E.; Kelton, K. F. Effects of microalloying with 3d transition metals on glass formation in AlYFe alloys. J. Non-cryst. Solids 2007, 353, 4723–4731.2
- 7. Shen, Y.; Perepezko, J. H. Al-based amorphous alloys: Glass-forming ability, crystallization behavior and effects of minor alloying additions. J. Alloy. Compd. 2017, 707, 3-11.
- 8. Zhuravlev, E.; Schick, C. Fast scanning power compensated differential scanning nano-calorimeter: 1. The device. Thermochim. Acta 2010, 505, 1-13.
- Zhuravlev, E.; Schick, C. Fast scanning power compensated differential scanning nano-calorimeter: 2. Heat capacity analysis. *Thermochim. Acta* **2010**, 505, 14-21.
- Inoue, A.; Matsumoto, N.; Masumoto, T. Al-Ni-Y-Co Amorphous Alloys with High Mechanical Strengths, Wide Supercooled Liquid Region and Large Glass-Forming Capacity. Mater. Trans. JIM 1990, 31, 493-500.
- Ye, F.; Lu, K. Crystallization kinetics of Al-La-Ni amorphous alloy. J. Non-Cryst. Solids 2000, 262, 228-235.
- Wang, J. Q.; Liu, Y. H.; Imhoff, S.; Chen, N.; Louzguine-Luzgin, D. V.; Takeuchi, A.; Chen, M. W.; Kato, H.; Perepezko, J. H.; Inoue, A. Enhance the thermal stability and glass forming ability of Al-based metallic glass by Ca minor-alloying. Intermetallics 2012, 29, 35-40.
- 13. Kelton, K. F.; Greer, A. L. Transient nucleation effects in glass formation. J. Non-Cryst. Solids 1986, 79, 295-309.
- Fokin, V. M.; Kalinina, A. M.; Filipovich, V. N. Nucleation in silicate glasses and effect of preliminary heat treatment on it. J. *Cryst. Growth* **1981**, 52, 115-121.1
- Lu, Z. P.; Liu, C. T. A new glass-forming ability criterion for bulk metallic glasses. Acta Mater. 2002, 50, 3501–3512.
- Perepezko, J.H. Nucleation-controlled reactions and metastable structures. Prog. Mater. Sci. 2004, 49, 263-284.
- Perepezko, J.H.; Imhoff, S.D. Primary crystallization reactions in Al-based metallic glass alloys. J. Alloys Compd. 2010, 504, S222-S225.
- 18. Zhang, B.; Zhao, D. Q.; Pan, M. X.; Wang, W. H.; Greer, A. L. Amorphous Metallic Plastic. Phys. Rev. Lett. 2005, 94, 205502.
- Johnson, W.L. Bulk Glass-Forming Metallic Alloys: Science and Technology. MRS Bull. 1999, 24, 42-56.

665

675

670

> 681 682 683

680

684 685

686 687

689 690 691

692 693 694

695 696 697

> 700 701 702

698

699

703 704

705 706

707 708

709 710 711

712 713

714 715

716 717

- 20. Shen, Y.; Perepezko, J. H. The effect of minor addition of insoluble elements on transformation kinetics in amorphous Al alloys. *J. Alloys. Compd.* **2015**, 643, S260-S264.
- 21. Xing, L. Q.; Mukhopadhyay, A.; Buhro, W. E.; Kelton, K. F. Improved Al-Y-Fe glass formation by microalloying with Ti. *Philos. Mag. Lett* **2004**, 84, 293-302
- 22. Shen, Y.; Perepezko, J.H. Investigation of the nucleation delay time in Al-based metallic glasses by high rate calorimetry. *J. Non-cryst. Solids* **2018**, 502, 9-14.
- 23. Gao, M.; Perepezko, J. H. Flash DSC determination of the delay time for primary crystallization and minor alloying effect in marginal Al-based metallic glasses. *Thermochim. Acta* **2019**, 677, 91-98.
- 24. Slipenyuk, A.; Eckert, J. Correlation between enthalpy change and free volume reduction during structural relaxation of Zr55Cu30Al10Ni5 metallic glass. *Scr. Mater.* **2004**, 50, 39-441
- 25. Mei, J. N.; Soubeyroux, J. L.; Blandin, J. J.; Li, J. S.; Kou, H. C.; Fu, H. Z.; Zhou, L. Structural relaxation of Ti40Zr25Ni8Cu9Be18 bulk metallic glass. J. Non-cryst. Solids 2011, 357, 110-1151
- 26. Qiao, J. C.; Pelletier, J. M.; Blandin, J. J.; Gravier, S. High temperature deformation in a lanthanum based bulk metallic glass showing a pronounced secondary relaxation. *Mater. Sci. Eng. A* **2013**, 586, 57-61.
- 27. Men, H.; Kim, D. H. Fabrication of ternary Mg-Cu-Gd bulk metallic glass with high glass-forming ability under air atmosphere. *J. Mater. Res.* **2003**, 18, 1502-1504.
- 28. Mileva, D.; Androsch, R.; Zhuravlev, E.; Schick, C.; Wunderlich, B. Homogeneous nucleation and mesophase formation in glassy isotactic polypropylene. *Polymer* **2012**, 53, 277-282.
- 29. Onishi, Y.; Nakai, T. Effect of nucleation of Poly (1, 4-butylene terephthalate) on its flowability. *Polymer J. Calorim.* **1992**, 24, 833-840
- 30. H. Tanaka. Importance of many-body orientational correlations in the physical description of liquids. *Faraday Discuss.* **2013**, 167, 9-76
- 31. S. Wouters, F. Demir, L. Beenaerts, and G. V. Assche. Calibration and performance of a fast-scanning DSC—Project RHC. *Thermochim. Acta* **2012**, 530, 64-72.
- 32. J. Jiang, E. Zhuravlev, Z. Huang, L. Wei, Q. Xu, M. Shan, G. Xue, D. Zhou, C. Schick, and W. Jiang. A transient polymorph transition of 4-cyano-4'-octyloxybiphenyl (8OCB) revealed by ultrafast differential scanning calorimetry (UFDSC). *Soft Matter*. **2013**, *9*, 1488-1491.
- 33. K. Six, G. Verreck, J. Peeters, K. Binnemans, and H. Berghmans. Investigation of thermal properties of glassy itraconazole: identification of a monotropic mesophase. *Thermochim. Acta* **2001**, 376, 175-181
- 34. M. Tarnacka, K. Adrjanowicz, E. Kaminska, K. Kaminski, K. Grzybowska, K. Kolodziejczyk, P. Wlodarczyk, L. Hawelek, G. Garbacz, A. Kocot, and M. Paluch. Molecular dynamics of itraconazole at ambient and high pressure. *Phys. Chem. Chem. Phys.* **2013**,15, 20742-20752
- 35. J. J. M. Ramos and H. P. Diogo. The slow relaxation dynamics in active pharmaceutical ingredients studied by DSC and TSDC: Voriconazole, miconazole and itraconazole. *Int. J. Pharmacol.* **2016**, 501, 39-48.
- 36. Broadband Dielectric Spectroscopy edited by F. Kremer and A. Schönhals (Springer, Berlin, 2003).
- 37. Y. González, B. Palacios, M. A. P. Jubindo, M. R. de la Fuente, and J. L. Serrano. Dielectric relaxation study in a glassy low-molecular-weight ferroelectric liquid crystal. *Phys. Rev. E* **1995**, 52, R5764.
- 38. A. R. Brás, M. Dionísio, H. Huth, C. Schick, and A. Schönhals. Origin of glassy dynamics in a liquid crystal studied by broadband dielectric and specific heat spectroscopy. *Phys. Rev. E* **2007**, 75, 061708.
- 39. A. Schönhals, H. L. Zubowa, R. Fricke, S. Frunza, L. Frunza, and R. Moldovan. On the Dielectric Behavior of Unaligned Samples of 4-n-Octyl-4'-cyanobiphenyl (8CB). *Cryst. Res. Technol.* **1999**, 34, 1309.
- 40. M. Tarnacka, K. Adrjanowicz, E. Kaminska, K. Kaminski, K. Grzybowska, K. Kolodziejczyk, P. Wlodarczyk, L. Hawelek, G. Garbacz, A. Kocot, and M. Paluch. Molecular dynamics of itraconazole at ambient and high pressure. *Phys. Chem. Chem. Phys.* **2013**, 15, 20742-20752.
- 41. E. U. Mapesa, M. Tarnacka, E. Kaminska, K. Adrjanowicz, M. Dulski, W. Kossack, M. Tress, W. K. Kipnusu, K. Kaminski, and F. Kremer. Molecular dynamics of itraconazole confined in thin supported layers. *RSC Adv.* **2014**, 4, 28432-28438.